

Convexity Meets Curvature: Lifted Near-Field Super-Resolution

Sajad Daei, Gábor Fodor, Mikael Skoglund
 KTH Royal Institute of Technology, Stockholm, Sweden
 {sajado,gaborf,skoglund}@kth.se

Abstract—Extra-large apertures, high carrier frequencies, and integrated sensing and communications (ISAC) are pushing array processing into the Fresnel region, where spherical wavefronts induce a range-dependent phase across the aperture. This curvature breaks the Fourier/Vandermonde structure behind classical subspace methods, and it is especially limiting with hybrid front-ends that provide only a small number of pilot measurements. Consequently, practical systems need continuous-angle resolution and joint angle-range inference where many near-field approaches still rely on costly 2D gridding. We show that *convexity can meet curvature* via a lifted, gridless super-resolution framework for near-field measurements. The key is a Bessel-Vandermonde factorization of the Fresnel-phase manifold that exposes a hidden Vandermonde structure in angle while isolating the range dependence into a compact coefficient map. Building on this, we introduce a lifting that maps each range bin and continuous angle to a structured rank-one atom, converting the nonlinear near-field model into a linear inverse problem over a row-sparse matrix. Recovery is posed as atomic-norm minimization and an explicit dual characterization via bounded trigonometric polynomials yields certificate-based localization that super-resolves off-grid angles and identifies active range bins. Simulations with strongly undersampled hybrid observations validate reliable joint angle-range recovery for next-generation wireless and ISAC systems.

Index Terms—Near-field, super-resolution, optimization, XL-MIMO arrays, atomic norm minimization, ISAC.

I. INTRODUCTION

Near-field arrays and loss of Fourier structure: The steady growth of array apertures in emerging wireless systems, driven by higher carrier frequencies, tighter spectrum reuse, and the convergence of communication with sensing, is reshaping the operating regime of multi-antenna signal processing. When the aperture becomes electrically large, many scatterers and targets of interest lie in the near field of the array. In this regime, the received field is more accurately described by spherical wavefronts rather than plane waves. As a consequence, the phase variation across the array depends not only on the direction of arrival but also on the propagation distance, and the far-field Fourier model that supports classical beampulse processing no longer applies [1]–[3]. This change has practical and conceptual implications. Practically, hybrid analog-digital architectures typically expose only a small number of linear measurements per pilot snapshot, so near-field estimation must succeed in a strongly undersampled regime. Conceptually, near-field responses do not admit a

This work is supported in part by Digital Futures. G. Fodor was also supported by SSF grant FUS21-0004 SAICOM and the EU Horizon 2023 project 6G-MUSICAL (Project ID: 101139176).

simple Fourier dictionary: the curvature-induced phase profile is range-dependent and interacts with direction in a way that destroys the shift-invariance and Vandermonde properties that many estimators rely on. These challenges are amplified in multi-path environments where several components may be closely spaced in direction yet separated in range (or vice versa), precisely the scenario where super-resolution is most valuable [4]–[6].

Limitations of existing methods: A common response to near-field modeling is to discretize both range and angle and apply sparse recovery with a two-dimensional dictionary [2], [7]–[9]. While conceptually straightforward, this strategy inherits two well-known difficulties. First, grid mismatch can dominate performance: in high-resolution regimes the true parameters rarely align with the discretization, causing bias and leakage that are difficult to control. Second, the computational burden grows rapidly with grid refinement, and becomes particularly acute when the estimation must be repeated across orthogonal frequency division multiplexing (OFDM) subcarriers or time slots [10]. Beyond 2D gridding, two representative classes of near-field estimators still leave important gaps. First, a recent gridless alternative [11] combines a second-order Taylor approximation with an atomic-norm program; however, its convexification relies on an auxiliary low-dimensional modulation/subspace model that represents the near-field phase variation through an *unknown waveform*. This adds a non-physical tuning burden (subspace dimension/structure) not uniquely dictated by the near-field manifold, and it can affect identifiability, estimation accuracy, and computational cost. Second, many practical solutions resort to local approximations of the spherical model and iterative nonlinear fitting. Such methods can be sensitive to initialization, degrade when components are closely spaced, and become fragile under compressed measurements. Crucially, neither class provides a unified *certificate-based* mechanism, in the sense of dual-polynomial/convex-geometry optimality conditions—that guarantees stable recovery of continuous parameters under undersampling [6], [12], [13].

Proposed approach: linearize by lifting, then super-resolve. This paper develops a different approach that restores the linear inverse-problem structure while respecting near-field physics. The key idea is to convert the near-field array manifold into a representation that is linear in a lifted domain. Instead of forcing the near-field response into a far-field dictionary or discretizing the angular domain, we exploit a harmonic expansion that reveals a hidden Vandermonde structure in angle, coupled to range-dependent coefficients. This factoriza-

tion enables a lifting procedure that maps each propagation path to a simple structured matrix atom. In the lifted domain, hybrid pilot measurements become linear functionals of a low-complexity superposition of such atoms. Once the model is linearized, the problem becomes amenable to gridless convex super-resolution. In particular, an atomic norm built from lifted near-field atoms provides a principled convex surrogate for the number of paths, and its dual yields explicit trigonometric-polynomial certificates that localize continuous angles. This connects near-field channel estimation to the broader theory of continuous compressed sensing and super-resolution [4], [6], [12]–[14], while introducing new structure specific to spherical-wave propagation.

A. Contributions

Our contributions establish a principled bridge between near-field wave physics and gridless convex super-resolution under compressed measurements:

- 1) **Physics-to-harmonics: a near-field manifold with a hidden Vandermonde core.** We develop a Bessel-Vandermonde harmonic representation of the Fresnel-region steering vector that isolates range dependence into a compact coefficient map while preserving a Vandermonde structure in angle. This representation explains *how and where* curvature creates additional harmonics beyond the far-field model, and it collapses to the classical far-field steering vector as range goes to infinity.
- 2) **Lifted linearization: from nonlinear Fresnel geometry to a structured linear inverse problem.** Leveraging the harmonic model, we introduce a lifting that maps each (discretized) range bin and continuous angle to a rank-one, row-sparse matrix atom. This yields a linear measurement model for hybrid-combined pilots, turning near-field joint angle-range estimation into a convex-amenable inverse problem with explicit structure (row sparsity across range and continuous sparsity in angle).
- 3) **Gridless recovery with certificates: atomic norms and dual-polynomial localization.** We pose reconstruction as atomic-norm minimization over the lifted atoms and provide an explicit dual characterization via bounded trigonometric polynomials. The resulting certificate-based peak rule identifies active range bins and *super-resolves* off-grid angles without angular discretization.
- 4) **Amplitude estimation via simple least-squares.** Given the estimated supports, path gains are obtained in closed-form by solving a simple least-square (LS) optimization which results in a complete complex-amplitude estimate with negligible additional computational cost.

Notation: \mathbf{I}_N is the $N \times N$ identity matrix; \mathbb{Z} and \mathbb{Z}_+ denote integers and positive integers. \otimes means Kronecker product. For $\mathbf{X} \in \mathbb{C}^{M \times N}$, $\text{vec}(\mathbf{X}) \in \mathbb{C}^{MN \times 1}$ stacks columns and $\text{vec}^{-1}(\cdot)$ is its inverse. $\mathbf{A}[k, \ell]$ is the (k, ℓ) -th entry of \mathbf{A} , and $x[k]$ is the k -th entry of \mathbf{x} . We use paired indexing via a fixed bijection $p(\ell, q) : \mathcal{I} \rightarrow \{1, \dots, P\}$ (e.g., $\mathcal{I} = [-I_1, I_1] \times [-I_2, I_2]$) and write $A[n, (\ell, q)] \triangleq A[n, p(\ell, q)]$. $a_{\text{NF}}(r, \theta)[n]$ denotes the n -th entry of the near-field steering vector $\mathbf{a}_{\text{NF}}(r, \theta)$. $J_n(\cdot)$ is the Bessel function of the first kind, and \mathbf{e}_n is the n -th

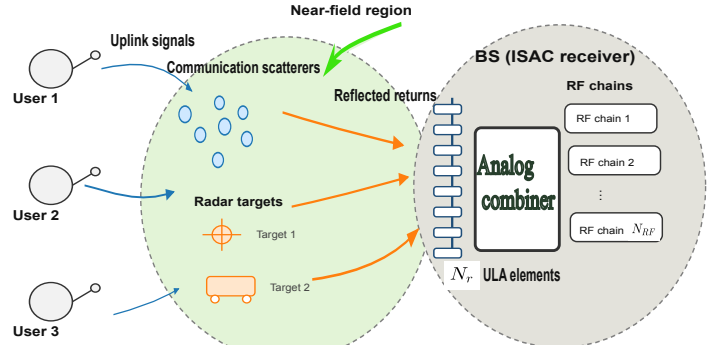


Figure 1. Hybrid XL-MIMO geometry with Analog combiner: a large-aperture BS observes a superposition of spherical-wave paths from multiple single-antenna uplink users and nearby targets/scatterers.

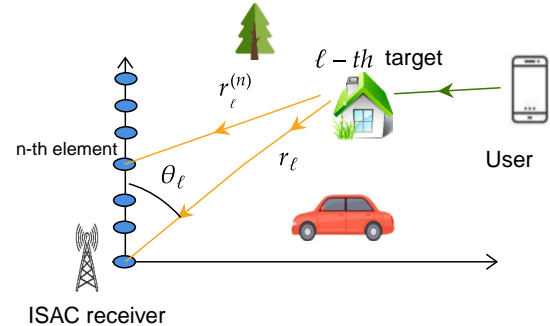


Figure 2. The uplink channel is comprised of L scatterers or targets. Each scatterer has a distinct range and angle parameter relative to the reference antenna with antenna element index $n = 0$.

canonical basis vector. $\langle \cdot, \cdot \rangle$ is the inner product of two vectors or matrices.

II. SYSTEM MODEL

A. Uplink pilot measurements with hybrid combining

We consider an uplink time-division duplexing (TDD) extra-large multiple-input multiple-output (XL-MIMO) OFDM system where the BS employs a uniform linear array (ULA) with N_r antennas and $N_{\text{RF}} \ll N_r$ RF chains with spacing $d = \lambda_c/2$ where $\lambda_c = \frac{c}{f_c}$ denotes the carrier wavelength and f_c is the carrier frequency as shown in Figure 1. In time slot p , the BS applies an analog combiner $\mathbf{B}_p \in \mathbb{C}^{N_{\text{RF}} \times N_r}$ with constant-modulus entries $|\mathbf{B}_p(i, j)| = \frac{1}{\sqrt{N_r}}$ [15]. For a given user and subcarrier, let $\mathbf{h} \in \mathbb{C}^{N_r \times 1}$ denote the uplink channel. With pilot symbol x_p (set to 1 for simplicity), the received measurement is $\mathbf{y}_p = \mathbf{B}_p \mathbf{h} x_p + \mathbf{B}_p \mathbf{w}_p$, $\mathbf{w}_p \sim \mathcal{CN}(\mathbf{0}, \sigma^2 \mathbf{I}_{N_r})$. Stacking P_T slots and setting $x_p = 1$ yields

$$\mathbf{y} = \mathbf{Bh} + \mathbf{Bw} \in \mathbb{C}^M, \quad M \triangleq P_T N_{\text{RF}}, \quad (1)$$

where $\mathbf{B} \triangleq [\mathbf{B}_1^\top, \dots, \mathbf{B}_{P_T}^\top]^\top \in \mathbb{C}^{M \times N_r}$ and $\mathbf{w} \triangleq [\mathbf{w}_1^\top, \dots, \mathbf{w}_{P_T}^\top]^\top$. The effective noise \mathbf{Bw} is colored with covariance $\mathbf{C}_w \triangleq \mathbb{E}[(\mathbf{Bw})(\mathbf{Bw})^\top]$. Let \mathbf{L}_{chol} denote the (lower-triangular) Cholesky factor of \mathbf{C}_w , i.e., $\mathbf{C}_w = \sigma^2 \mathbf{L}_{\text{chol}} \mathbf{L}_{\text{chol}}^\top$. Pre-whitening gives the equivalent model (see e.g. [7], [15]):

$$\mathbf{y}' = \mathbf{B}' \mathbf{h} + \mathbf{w}', \quad (2)$$

where $\mathbf{y}' \triangleq \mathbf{L}_{\text{chol}}^{-1} \mathbf{y}$, $\mathbf{B}' \triangleq \mathbf{L}_{\text{chol}}^{-1} \mathbf{B}$, and $\mathbf{w}' \triangleq \mathbf{L}_{\text{chol}}^{-1} \mathbf{Bw} \sim \mathcal{CN}(\mathbf{0}, \sigma^2 \mathbf{I}_M)$.

B. Near-field channel model

We adopt a sparse near-field model with L dominant paths. These paths may be communications scatterers or radar targets as shown in Figures 1 and 2. The uplink channel can be expressed as:

$$\mathbf{h} = \sum_{\ell=1}^L c_{\ell} \mathbf{a}_{\text{NF}}(r_{\ell}, \theta_{\ell}) \quad c_{\ell} \in \mathbb{C}, \quad (3)$$

where $(r_{\ell}, \theta_{\ell})$ denotes the range and azimuth angle of path ℓ w.r.t. a reference antenna (antenna $n = 0$). Amplitude variations across antennas are absorbed into c_{ℓ} .

Let d be the antenna spacing and index antennas by $n \in \{0, 1, \dots, N_r - 1\}$. Define the distance from the scatterer at polar coordinates (r, θ) to antenna n as

$$r^{(n)} \triangleq \sqrt{r^2 + (nd)^2 - 2r(nd) \cos \theta}. \quad (4)$$

We define the near-field steering vector (up to a global phase) as

$$\mathbf{a}_{\text{NF}}(r, \theta)[n] \triangleq \exp\left(-jk_{\lambda}(r^{(n)} - r)\right), \quad n = 0, \dots, N_r - 1, \quad (5)$$

where $k_{\lambda} \triangleq \frac{2\pi}{\lambda}$. The goal is *Given \mathbf{y}' and \mathbf{B}' , estimate $\{(r_{\ell}, \theta_{\ell}, c_{\ell})\}_{\ell=1}^L$ with continuous angles θ_{ℓ} .*

III. BESSEL-VANDERMONDE LIFTING AND LINEAR MEASUREMENT MODEL

In the following theorem, we provide a lifted Bessel-Vandermonde approximation of the near-field steering vector. This provides a way that the near-field steering vector, which is generally nonlinear in the parameters, can be stated as a linear and deterministic functional of a higher dimensional row-sparse matrix.

Theorem 1. Consider a ULA with $N_r \geq 2$ antennas indexed by $n = 0, \dots, N_r - 1$ and spacing d . Let $(r, \theta) \in [r_{\min}, r_{\max}] \times (0, \pi)$ be the polar coordinates of a communication scatterer or radar target. Assume $r_{\min} > 0$ and define $z_1(n) \triangleq k_{\lambda}nd$, $z_2(n, r) \triangleq k_{\lambda} \frac{n^2 d^2}{4r}$. Fix truncation orders $I_1, I_2 \in \mathbb{Z}_+$ and set $P \triangleq (2I_1+1)(2I_2+1)$, $I_{\text{off}} \triangleq I_1 + 2I_2$, $N_b \triangleq 2I_{\text{off}} + 1$. Define the normalized Vandermonde vector

$$\tilde{\mathbf{v}}(\theta) \triangleq \frac{1}{\sqrt{N_b}} [e^{-jI_{\text{off}}\theta}, \dots, e^{jI_{\text{off}}\theta}]^T \in \mathbb{C}^{N_b \times 1} \quad (6)$$

Let $p(\ell, q)$ be any bijection from $[-I_1, I_1] \times [-I_2, I_2]$ to $\{1, \dots, P\}$. Define $\mathbf{S} \in \{0, 1\}^{P \times N_b}$ by $S[p(\ell, q), \ell+2q+I_{\text{off}}+1] = 1$ and zeros otherwise, so each row of \mathbf{S} contains exactly one nonzero entry. For each $r > 0$, define $\mathbf{C}(r) \in \mathbb{C}^{N_r \times P}$ row-wise by

$$C(r)[n, (\ell, q)] \triangleq e^{-jz_2(n, r)} j^{\ell+q} J_{\ell}(z_1(n)) J_q(z_2(n, r)), \quad |\ell| \leq I_1, \quad |q| \leq I_2. \quad (7)$$

Fix a range grid $\{r_i\}_{i=1}^{N_d}$ and define the dictionary

$$\mathbf{D} \triangleq [\text{vec}(\mathbf{C}(r_1)) \dots \text{vec}(\mathbf{C}(r_{N_d}))] \in \mathbb{C}^{N_r P \times N_d}.$$

Let $\boldsymbol{\alpha} \in \{0, 1\}^{N_d}$ be one-sparse with $\alpha[i] = 1$ iff $r = r_i$, and define the lifted atom $\mathbf{A}(r, \theta) \triangleq \boldsymbol{\alpha} \tilde{\mathbf{v}}(\theta)^H \in \mathbb{C}^{N_d \times N_b}$. For each

antenna index $n = 0, \dots, N_r - 1$, define

$$\boldsymbol{\Phi}_n \triangleq \sqrt{N_b} \mathbf{D}^T (\mathbf{I}_P \otimes \mathbf{e}_{n+1}) \mathbf{S} \in \mathbb{C}^{N_d \times N_b}. \quad (8)$$

Then, for every $n = 0, \dots, N_r - 1$,

$$a_{\text{NF}}(r, \theta)[n] = \langle \mathbf{A}(r, \theta), \boldsymbol{\Phi}_n \rangle + \delta_n(r, \theta), \quad (9)$$

where the approximation error decomposes as

$$\delta_n(r, \theta) = \underbrace{\mathcal{O}\left(k_{\lambda} \frac{n^3 d^3}{r^3}\right)}_{\text{Fresnel remainder}} + \underbrace{\delta_n^{\text{tail}}(I_1, I_2)}_{\text{Bessel truncation tail}}. \quad (10)$$

with $|\delta_n^{\text{tail}}(I_1, I_2)| \leq \sum_{|\ell| > I_1} \sum_{q \in \mathbb{Z}} |J_{\ell}(z_1(n))| |J_q(z_2(n, r))| + \sum_{|q| > I_2} \sum_{\ell \in \mathbb{Z}} |J_{\ell}(z_1(n))| |J_q(z_2(n, r))|$.

Remark 1. (Interpretation) The theorem says that by *lifting* angle-distance pairs to the rank-one matrix \mathbf{A} , the inherently nonlinear near-field response becomes an *affine* functional of \mathbf{A} . This enables convex tools such as atomic-norm minimization and RIPless guaranties [6], [12]: recovery reduces to solving a linear inverse problem in the lifted space. \mathbf{S} is the selection matrix that selects the appropriate harmonics. We refer to \mathbf{A} as the “**lifted channel matrix**” and to the linear map $\boldsymbol{\Phi}(\cdot) = \{\boldsymbol{\Phi}_n\}_{n=0}^{N_r-1} : \mathbb{C}^{N_d \times N_b} \rightarrow \mathbb{C}^{N_r \times 1}$ as “**Bessel-Vandermonde operator**,” which encodes distance-domain Bessel terms and the angular Vandermonde structure.

Remark 2 (Far-field limit). As $r \rightarrow \infty$, $z_2(n, r) \rightarrow 0$ so $J_q(z_2(n, r)) \rightarrow 0$ for $q \neq 0$ and $J_0(z_2(n, r)) \rightarrow 1$. Hence only the $q = 0$ terms in (7) survive and the approximation reduces to the classical far-field steering vector

$$a_{\text{NF}}(r, \theta)[n] \rightarrow a_{\text{FF}}(\theta)[n] = \exp(jk_{\lambda}nd \cos \theta),$$

recovering the standard Vandermonde/Fourier structure.

If $I_1 \geq \left\lceil \frac{e\pi(N_r-1)d}{\lambda} \right\rceil$ and $I_2 \geq \left\lceil \frac{e}{2} \max_{0 \leq n \leq N_r-1} |z_2(n, r)| \right\rceil$ (and vanish as $I_1, I_2 \rightarrow \infty$), then the Bessel truncation tail can be made arbitrarily small. If $r \geq \sqrt{k_{\lambda}} ((N_r - 1)d)^{\frac{3}{2}}$, the the Fresnel remainder can become very small. In practice small truncation orders (e.g., $I_1 = 5, I_2 = 1$) suffice; see Section IV.

Based on Theorem 1 in the Fresnel region and with sufficiently large I_1, I_2 , we are now able to represent the near-field channel as follows: $h[n] \approx \langle \mathbf{X}, \boldsymbol{\Phi}_n \rangle$, $n = 0, \dots, N_r - 1$ where $\mathbf{A}_l = \boldsymbol{\alpha}_l \tilde{\mathbf{v}}^H(\theta_l)$ and $\mathbf{X} = \sum_{l=1}^L c_l \mathbf{A}_l$ is an unknown matrix depending on both angle and distance of the scatterers. The pilot measurements provided in (2) can also be expressed in this form:

$$\mathbf{y}' = \mathbf{B}'(\mathbf{X}) + \mathbf{w}' \in \mathbb{C}^{M \times 1}, \quad (11)$$

$$(\mathbf{B}'(\mathbf{X}))[m] \triangleq \langle \mathbf{X}, \boldsymbol{\Psi}_m \rangle, \quad m = 1, \dots, M. \quad (12)$$

where $\boldsymbol{\Psi}_m \triangleq \sum_{n=0}^{N_r-1} B'[m, n] \boldsymbol{\Phi}_n \in \mathbb{C}^{N_d \times N_b}$. The number of unknown variables in the latter lifted model is $N_d N_b$ while the number of known equations is $M \ll N_d N_b$. This makes the system of equations widely under-determined. Since our lifted matrix \mathbf{X} is actually a superposition of $L \ll \min\{N_d, N_b\}$ rank-one, row-sparse atoms $\boldsymbol{\alpha}_l \tilde{\mathbf{v}}^H(\theta_l)$, continuous compressed sensing or super-resolution methods [6], [12], [16] can indeed unlock exact recovery despite $M < N_d N_b$. To do so, note

that the matrix \mathbf{X} is composed of few matrix-valued atoms \mathbf{A}_l . Since the distance vector $\boldsymbol{\alpha} \in \mathbb{R}^{N_d \times 1}$ is one-sparse, the resultant matrix $\mathbf{A} = \boldsymbol{\alpha} \tilde{\mathbf{v}}^H(\theta)$ is both row-sparse and rank one. In fact, $\mathbf{A}_l = \boldsymbol{\alpha} \tilde{\mathbf{v}}^H(\theta)$ is an *atom* or building block from the atomic set

$$\mathcal{A} = \{\boldsymbol{\alpha} \tilde{\mathbf{v}}^H(\theta) \in \mathbb{C}^{N_d \times N_b} : \theta \in [0, 2\pi), \|\boldsymbol{\alpha}\|_1 = 1, \boldsymbol{\alpha} \in \{0, 1\}^{N_d \times 1}\}$$

Note that since $\boldsymbol{\alpha} \in \{0, 1\}^{N_d \times 1}$, we have that $\|\boldsymbol{\alpha}\|_1 = \|\boldsymbol{\alpha}\|_0$. To promote row-sparsity and rank-one structure of \mathbf{X} jointly, we define the following atomic function:

$$\|\mathbf{X}\|_{\mathcal{A}} = \inf\{t \geq 0 : \mathbf{X} \in t\text{conv}(\mathcal{A})\} = \inf_{c_l} \{\sum_l |c_l| : \mathbf{X} = \sum_{l=1}^L c_l \mathbf{A}(r_l, \theta_l)\}$$

where $\|\mathbf{X}\|_{\mathcal{A}}$ is called the *atomic* norm [6], [12], [13] and is the closest convex surrogate to “number of lifted atoms”, encouraging few active range bins and a sparse continuous angular spectrum per bin. By minimizing this function subject to satisfying some measurement constraints, one can recover this matrix. This is done in the following optimization:

$$\min_{\mathbf{Z} \in \mathbb{C}^{N_d \times N_b}} \|\mathbf{Z}\|_{\mathcal{A}} \text{ s.t. } \|\mathbf{y} - \mathcal{B}'(\mathbf{Z})\|_2 \leq \eta \quad (13)$$

where η is an upper-bound for $\|\mathbf{w}'\|_2$ in (2). The dual of the latter optimization problem can be obtained as follows (see e.g. [4], [14], [17]–[20]):

$$\max_{\mathbf{q}} \text{Re}\langle \mathbf{y}, \mathbf{q} \rangle - \eta \|\mathbf{q}\|_2 \text{ s.t. } \|\mathcal{B}'^{\text{Adj}}(\mathbf{q})\|_{\mathcal{A}}^d \leq 1, \quad (14)$$

where $\|\mathbf{X}\|_{\mathcal{A}}^d \triangleq \sup_{\|\mathbf{Z}\|_{\mathcal{A}} \leq 1} \langle \mathbf{X}, \mathbf{Z} \rangle = \sup_{\theta \in (0, \pi)} \langle \boldsymbol{\alpha} \tilde{\mathbf{v}}^H(\theta), \mathbf{Z} \rangle = \sup_{\theta} \|\mathbf{Z}^H \tilde{\mathbf{v}}(\theta)\|_{\infty}$ is called the dual atomic norm and $\mathcal{B}'^{\text{Adj}}(\mathbf{q}) = \sum_{m=1}^M q_m \Psi_m \in \mathbb{C}^{N_d \times N_b}$, is the adjoint operator of $\mathcal{B}'(\cdot)$. The following lemma provides a way to state the dual problem (14) in an equivalent tractable semidefinite programming (SDP) form.

Lemma 1. Let $\Psi_m \triangleq \left[\psi_m^1, \dots, \psi_m^{N_d} \right]^T \in \mathbb{C}^{N_d \times N_b}$ and $\tilde{\Psi}_i = \left[\psi_1^i \dots \psi_M^i \right] \in \mathbb{C}^{N_b \times M} \forall i = 1, \dots, N_d$. Then, the dual optimization problem (14) can be relaxed to the following SDP optimization problem

$$\begin{aligned} & \max_{\mathbf{Q}_i \in \mathbb{C}^{N_b \times N_b}, \mathbf{q} \in \mathbb{C}^{M \times 1}} \text{Re}\langle \mathbf{y}, \mathbf{q} \rangle - \eta \|\mathbf{q}\|_2 \\ & \text{s.t. } \begin{bmatrix} \mathbf{Q}_i & \tilde{\Psi}_i \mathbf{q} \\ \mathbf{q}^H \tilde{\Psi}_i^H & 1 \end{bmatrix} \succeq \mathbf{0} \forall i = 1, \dots, N_d, \end{aligned} \quad (15)$$

$$\langle \Theta_n, \mathbf{Q}_i \rangle = 1_{n=0}, n = -N_b + 1, \dots, N_b - 1, \quad (16)$$

where Θ_n is the elementary Toeplitz matrix with ones along its n -th diagonal and zero elsewhere.

Define range-indexed dual polynomials $p_i(\theta) \triangleq e_i^T \mathcal{B}'^{\text{Adj}}(\mathbf{q}) \tilde{\mathbf{v}}(\theta)$, $i = 1, \dots, N_d$. At optimum, peaks of $|p_i(\theta)|$ identify the active range bins and continuous angles as shown in Figure 3a. Moreover, the support is recovered by $\hat{\mathcal{S}} = \{(i, \theta) : |p_i(\theta)| = 1\} = \{(i_\ell, \theta_\ell)\}_{\ell=1}^{\hat{L}}$. Insert the estimated support $\hat{\mathcal{S}} = (\hat{r}_\ell, \hat{\theta}_\ell)_{\ell=1}^{\hat{L}}$ into (11) and estimate the gains by an LS debiasing step (cf. [4, Eq. 29]). Define $\mathbf{G} \in \mathbb{C}^{M \times \hat{L}}$ with $G[m, \ell] \triangleq \langle \mathbf{A}(\hat{r}_\ell, \hat{\theta}_\ell), \Psi_m \rangle_F$, then $\hat{\mathbf{c}} = \arg \min_{\mathbf{c}} \|\mathbf{y}' - \mathbf{G}\mathbf{c}\|_2^2 = (\mathbf{G}^H \mathbf{G})^{-1} \mathbf{G}^H \mathbf{y}'$.

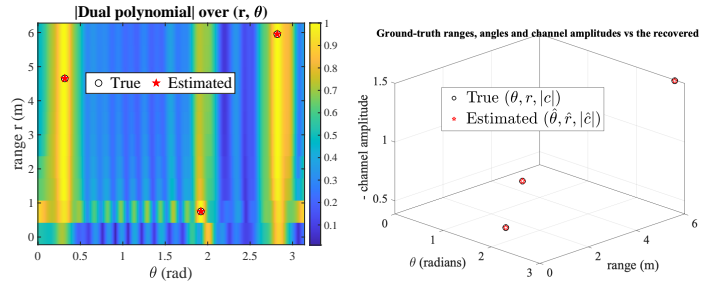


Figure 3. Gridless recovery outputs: (a) dual polynomial used for localization, (b) recovered amplitudes. The estimates $\hat{r}_\ell, \hat{\theta}_\ell$ and \hat{c}_ℓ are precisely aligned with the ground-truth ones.

IV. NUMERICAL EXPERIMENTS

We validate (i) the truncated Bessel-Vandermonde lifting and (ii) the gridless dual-certificate localization. A ULA with $N_r = 64$ antennas and spacing $d = \lambda/2$ is simulated at $f_c = 100$ GHz. We use a range grid of $N_d = 10$ bins uniformly spanning $[r_{\min}, r_{\max}] = [0.1, 6]$ m and generate $L = 3$ near-field paths with random (r_ℓ, θ_ℓ) selected on the grid and $\theta_\ell \sim \text{Unif}(0, \pi)$, with different gains. The near-field steering vectors are computed both from the exact spherical model (5) and from the truncated Jacobi-Anger expansion with $(I_1, I_2) = (5, 1)$. We observe that both the Fresnel and Bessel tail terms are negligible. To demonstrate gridless recovery, we solve the dual SDP in Lemma 1 (CVX/SDPT3) and evaluate the range-indexed dual polynomials on a fine angular grid. Peaks of $|p_i(\theta)|$ identify the active range bins and continuous angles (Fig. 3(a)). Given the estimated supports, the complex path gains are obtained by a least-squares fit using the reconstructed atoms (Fig. 3(b)). As it turns out from Figures 3a and 3b, the range, angle and path gain estimates perfectly match the ground-truth ones.

V. CONCLUSION

This work delivers a simple message for near-field XL-MIMO/ISAC: losing Fourier structure does not require 2D gridding or fragile nonlinear fitting. By exposing a *hidden* Vandermonde core in the Fresnel manifold via a Bessel-Vandermonde expansion and lifting range-angle pairs to structured rank-one atoms, we turn near-field geometry into a linear inverse problem that is compatible with compressed pilots. This is more than a modeling convenience: it enables a fully gridless convex program whose dual polynomials act as verifiable certificates for localization. Continuous angles are super-resolved while active range bins are revealed by row support; path gains follow from closed-form least-squares post-processing. Beyond robust performance under strong undersampling, the framework provides a unifying view across propagation regimes: as curvature vanishes, it reduces to classical far-field super-resolution. The resulting Bessel-Vandermonde operator and certificate-based localization rule form a reusable building block for near-field signal processing, including wideband and multi-user extensions and joint communication-sensing scenarios, where hybrid hardware makes each measurement highly valuable.

VI. PROOF OF THEOREM 1

Let $r^{(n)} = r\sqrt{1+u}$, $u \triangleq \left(\frac{nd}{r}\right)^2 - 2\left(\frac{nd}{r}\right)\cos\theta$. For fixed $r \geq r_{\min}$ and $n \leq N_r - 1$, we have $|u| \leq 2\frac{nd}{r} + \left(\frac{nd}{r}\right)^2$. Using Taylor's theorem for $\sqrt{1+u}$ around $u = 0$, i.e., $\sqrt{1+u} = 1 + \frac{u}{2} - \frac{u^2}{8} + \mathcal{O}(|u|^3)$, we have

$$r^{(n)} - r = r\left(\frac{u}{2} - \frac{u^2}{8}\right) + r\rho(u) = -nd\cos\theta + \frac{n^2d^2}{2r}\sin^2\theta + \varepsilon_n(r, \theta),$$

with $|\varepsilon_n(r, \theta)| = \mathcal{O}(\frac{(nd)^3}{r^3})$. Using $\sin^2\theta = \frac{1-\cos(2\theta)}{2}$ yields the standard Fresnel form $r^{(n)} - r = -nd\cos\theta + \frac{n^2d^2}{4r}(1 - \cos(2\theta)) + \varepsilon_n(r, \theta)$. Substituting into the definition of a_{NF} gives

$$a_{\text{NF}}(r, \theta)[n] = \exp(jz_1(n)\cos\theta) \exp(-jz_2(n, r)(1 - \cos(2\theta))) \exp(-jk\lambda\varepsilon_n(r, \theta)). \quad (17)$$

Define the Fresnel-approximated entry by dropping the last factor:

$$a_{\text{F}}(r, \theta)[n] \triangleq \exp(jz_1(n)\cos\theta) \exp(-jz_2(n, r)(1 - \cos(2\theta))).$$

Then, using $|e^{-jt} - 1| \leq |t|$, $|a_{\text{NF}} - a_{\text{F}}| = |a_{\text{F}}| \cdot |e^{-jk\lambda\varepsilon_n} - 1| \leq k\lambda|\varepsilon_n(r, \theta)|$ which proves the Fresnel remainder is $\mathcal{O}(k\lambda\frac{(nd)^3}{r^3})$. Rewrite the quadratic term as

$$\exp(-jz_2(1 - \cos(2\theta))) = e^{-jz_2} \exp(jz_2 \cos(2\theta)),$$

where $z_2 \triangleq z_2(n, r)$. By the Jacobi-Anger identity,

$$e^{jz_1 \cos\theta} = \sum_{\ell \in \mathbb{Z}} j^\ell J_\ell(z_1) e^{j\ell\theta}, e^{jz_2 \cos(2\theta)} = \sum_{q \in \mathbb{Z}} j^q J_q(z_2) e^{j2q\theta}.$$

Multiplying and using (17) (without the Fresnel remainder factor) yields the exact series

$$a_{\text{F}}(r, \theta)[n] = e^{-jz_2(n, r)} \sum_{\ell \in \mathbb{Z}} \sum_{q \in \mathbb{Z}} j^{\ell+q} J_\ell(z_1(n)) J_q(z_2(n, r)) e^{j(\ell+2q)\theta}. \quad (18)$$

Let $s_n(r, \theta)$ denote the truncated sum over $|\ell| \leq I_1$, $|q| \leq I_2$, and define the tail $\delta_n^{\text{tail}} \triangleq a_{\text{F}} - s_n$. Define $\mathbf{v}(\theta) \in \mathbb{C}^{P \times 1}$ with entries $v(\theta)[(\ell, q), 1] = e^{j(\ell+2q)\theta}$ for $|\ell| \leq I_1$, $|q| \leq I_2$. By construction of \mathbf{S} and $\tilde{\mathbf{v}}(\theta)$,

$$\mathbf{v}(\theta) = \sqrt{N_b} \mathbf{S} \tilde{\mathbf{v}}(\theta). \quad (19)$$

Also, by the definition of $\mathbf{C}(r)$ in (7), the truncated sum can be written as

$$s_n(r, \theta) = \sum_{|\ell| \leq I_1} \sum_{|q| \leq I_2} C(r)[n, (\ell, q)] v(\theta)[(\ell, q), 1] = \mathbf{c}_n(r)^T \mathbf{v}(\theta), \quad (20)$$

where $\mathbf{c}_n(r)^T$ is the n -th row of $\mathbf{C}(r)$. Using the standard row-extraction identity for column-wise vectorization,

$$\mathbf{c}_n(r) = (\mathbf{I}_P \otimes \mathbf{e}_{n+1}^T) \text{vec}(\mathbf{C}(r)).$$

On the range grid, $\text{vec}(\mathbf{C}(r)) = \mathbf{D}\boldsymbol{\alpha}$ by definition of \mathbf{D} and the one-sparsity of $\boldsymbol{\alpha}$. Combining with (19) gives

$$\begin{aligned} s_n(r, \theta) &= \text{vec}(\mathbf{C}(r))^T (\mathbf{I}_P \otimes \mathbf{e}_{n+1}) \sqrt{N_b} \mathbf{S} \tilde{\mathbf{v}}(\theta) \\ &= \boldsymbol{\alpha}^T \mathbf{D}^T (\mathbf{I}_P \otimes \mathbf{e}_{n+1}) \mathbf{S} \sqrt{N_b} \tilde{\mathbf{v}}(\theta) = \boldsymbol{\alpha}^T \boldsymbol{\Phi}_n \tilde{\mathbf{v}}(\theta), \end{aligned}$$

where $\boldsymbol{\Phi}_n$ is as in (8). Finally, for $\mathbf{A}(r, \theta) = \boldsymbol{\alpha} \tilde{\mathbf{v}}(\theta)^H$,

$$\langle \mathbf{A}(r, \theta), \boldsymbol{\Phi}_n \rangle = \text{Tr}(\mathbf{A}(r, \theta)^H \boldsymbol{\Phi}_n) = \text{Tr}(\tilde{\mathbf{v}}(\theta) \boldsymbol{\alpha}^T \boldsymbol{\Phi}_n) = \boldsymbol{\alpha}^T \boldsymbol{\Phi}_n \tilde{\mathbf{v}}(\theta) = s_n(r, \theta). \quad (21)$$

Thus $a_{\text{NF}}[n] = s_n + \delta_n^{\text{F}} + \delta_n^{\text{tail}}$, which is exactly (9).

REFERENCES

- [1] L. Lu, G. Y. Li, A. L. Swindlehurst, A. Ashikhmin, and R. Zhang, "An overview of massive MIMO: Benefits and challenges," *IEEE journal of selected topics in signal processing*, vol. 8, no. 5, pp. 742–758, 2014.
- [2] Y. Liu, C. Ouyang, Z. Wang, J. Xu, X. Mu, and A. L. Swindlehurst, "Near-field communications: A comprehensive survey," *IEEE Communications Surveys & Tutorials*, 2024.
- [3] S. Daei, G. Fodor, and M. Skoglund, "When near becomes far: From rayleigh to optimal near-field and far-field boundaries," *IEEE GLOBECOM*, 2025.
- [4] S. Daei, S. Razavikia, M. Skoglund, G. Fodor, and C. Fischione, "Timely and painless breakups: Off-the-grid blind message recovery and users' demixing," *IEEE Transactions on Information Theory*, 2025.
- [5] S. Daei, A. Zamani, S. Chatterjee, M. Skoglund, and G. Fodor, "Near-field isac in 6g: Addressing phase nonlinearity via lifted super-resolution," in *ICASSP 2025-2025 IEEE International Conference on Acoustics, Speech and Signal Processing (ICASSP)*. IEEE, 2025, pp. 1–5.
- [6] G. Tang, B. N. Bhaskar, P. Shah, and B. Recht, "Compressed sensing off the grid," *IEEE transactions on information theory*, vol. 59, no. 11, pp. 7465–7490, 2013.
- [7] M. Cui and L. Dai, "Channel estimation for extremely large-scale MIMO: Far-field or near-field?" *IEEE Transactions on Communications*, vol. 70, no. 4, pp. 2663–2677, 2022.
- [8] X. Zhang, Z. Wang, H. Zhang, and L. Yang, "Near-field channel estimation for extremely large-scale array communications: A model-based deep learning approach," *IEEE Communications Letters*, vol. 27, no. 4, pp. 1155–1159, 2023.
- [9] Z. Wang, X. Mu, and Y. Liu, "Near-field integrated sensing and communications," *IEEE Communications Letters*, vol. 27, no. 8, pp. 2048–2052, 2023.
- [10] Y. Chi, L. L. Scharf, A. Pezeshki, and A. R. Calderbank, "Sensitivity to basis mismatch in compressed sensing," *IEEE Transactions on Signal Processing*, vol. 59, no. 5, pp. 2182–2195, 2011.
- [11] F. Xi and D. Yang, "Near-field channel estimation and joint angle-range recovery in xl-mimo systems: A gridless super-resolution approach," *arXiv preprint arXiv:2511.23187*, 2025.
- [12] E. J. Candès and C. Fernandez-Granda, "Towards a mathematical theory of super-resolution," *Communications on pure and applied Mathematics*, vol. 67, no. 6, pp. 906–956, 2014.
- [13] V. Chandrasekaran, B. Recht, P. A. Parrilo, and A. S. Willsky, "The convex geometry of linear inverse problems," *Foundations of Computational mathematics*, vol. 12, no. 6, pp. 805–849, 2012.
- [14] S. Daei and M. Kountouris, "Blind goal-oriented massive access for future wireless networks," *IEEE Transactions on Signal Processing*, vol. 71, pp. 901–916, 2023.
- [15] A. Alkhateeb, O. El Ayach, G. Leus, and R. W. Heath, "Channel estimation and hybrid precoding for millimeter wave cellular systems," *IEEE journal of selected topics in signal processing*, vol. 8, no. 5, pp. 831–846, 2014.
- [16] C. Fernandez-Granda, "Super-resolution of point sources via convex programming," *Information and Inference: A Journal of the IMA*, vol. 5, no. 3, pp. 251–303, 2016.
- [17] S. Daei, S. Razavikia, M. Kountouris, M. Skoglund, G. Fodor, and C. Fischione, "Blind asynchronous goal-oriented detection for massive connectivity," in *2023 21st International Symposium on Modeling and Optimization in Mobile, Ad Hoc, and Wireless Networks (WiOpt)*. IEEE, 2023, pp. 167–174.
- [18] M. Safari, S. Daei, and F. Haddadi, "Off-the-grid recovery of time and frequency shifts with multiple measurement vectors," *Signal Processing*, vol. 183, p. 108016, 2021.
- [19] H. Maskan, S. Daei, and M. H. Kahaei, "Demixing sines and spikes using multiple measurement vectors," *Signal Processing*, vol. 203, p. 108786, 2023.
- [20] M. Seidi, S. Razavikia, S. Daei, and J. Oberhammer, "A novel demixing algorithm for joint target detection and impulsive noise suppression," *IEEE Communications Letters*, vol. 26, no. 11, pp. 2750–2754, 2022.